Numerical Investigation of Emission Properties and Pump Noise Transfer Functions of an Yb3+:Er3+:Tm3+:Ho3+ Co-Doped Glass

Numerical Investigation of Emission Properties and Pump Noise Transfer Functions of an Yb^{3+}:Er^{3+}:Tm^{3+}:Ho^{3+} Co-Doped Glass

Riccardo Ballarini and Stefano Taccheo

***Abstract*—Rare-earth doped glasses exhibit optical properties that depend on the specific rare-earth used, and therefore, rare-earth doped active devices are suitable for many different applications. In this article, for the first time to our knowledge, we investigate the emission, the gain spectrum and the properties of a 980-nm-pumped Yb^{3+}:Er^{3+}:Tm^{3+}:Ho^{3+} co-doped germanate glass. In such a complex quadruply-doped active glass, the pumping process operates via both direct pumping (to ytterbium and erbium) and energy transfer processes (ytterbium to the other three rare-earths, erbium to thulium and holmium and thulium to holmium), which also act as a de-excitation processes. The interplay of all processes relies on the relative rare-earth concentrations and the relative weights. The optimization study has been performed by means of a numerical model based on rate equation system, that takes into account eleven energy levels and relevant energy transfer phenomena between the different ions. The emission and gain properties have been studied at different rare-earth concentrations, in order to optimize the emission and gain spectra. With an optimal set of concentrations, a broadband emission spectrum with a proper power spectral density and a bandwidth at −10 dB of 660 nm has been achieved by joining the emission bandwidth of erbium at 1550 nm, thulium at 1800 nm and holmium at 2050 nm. Furthermore, the pump noise effect on the output of the system has been investigated by numerically calculating the pump noise transfer function. We show that thulium and holmium emission level populations are quite insensitive to pump intensity noise due to filtering by energy transfer processes.**

***Index Terms*—Emission spectrum, erbium, gain spectrum, holmium, optical amplifier, thulium, transfer function, ytterbium.**

I. Introduction

RARE-EARTH (RE) doped glass active materials are the core element of lasers, amplifiers and Amplified Spontaneous Emission (ASE) sources. The specific RE defines the emission and gain properties and the specific wavelength interval. Most commonly used RE materials include Ytterbium (Yb), Neodymium (Nd), Erbium (Er), Thulium (Tm) and Holmium (Ho), which allow emission from visible [1], [2], [3], [4], [5], [6] to infrared at 2 μm and above [6], [7], [8], [9], [10], [11], [12], [13], [14], [15], [16]. Applications includes lasers and optical amplifiers in many fields from material processing [17], sensing [5], [18], [19], [20], [21], medical applications [21], [22], [23], [24], [25], military [26], [27] and, in particular for amplifiers, telecommunication applications [15], [16], [28], [29], [30], [31]. One of the goals in several application areas is to improve efficiency and increase the emission or gain wavelength interval. To increase the wavelength emission bandwidth, multiple doping is a very attractive solution thanks to the possibility to obtain broadband emission and gain [7], [8], [9], [32], [33], [34] by overlap of emission from multiple RE ions.

Co-doped glasses using different combinations of two or three REs are present in several studies. Su et al. [35] realized an Yb^{3+}:Er^{3+}:Tm^{3+} co-doped tellurite glass, in which the thulium 1.8 μm emission band is well overlapped with the erbium 1.53 μm emission band, with a wide fluorescence spectrum approximately from 1500 nm to 2000 nm. Instead, Zhu et al. [36] tried to extend thulium band on the other side by the overlap with the 2 μm holmium emission, realizing a Tm^{3+}:Ho^{3+} co-doped tellurite glass with a Full Width Half Maximum (FWHM) of 360 nm. Other research groups [34], [37], [38] tried to mix emissions from these three REs, erbium, thulium and holmium, in order to obtain an ultra-broadband emission; in particular, Kochanowicz et al. [34] realized an Er^{3+}:Tm^{3+}:Ho^{3+} co-doped germanate glass fiber pumped at 976 nm, able to achieve an ASE emission bandwidth at −10 dB of 690 nm.

One of the key issue with multiple REs doping is to balance the different ion concentrations in order to obtain a homogeneous emission or gain spectrum and an efficient pumping. As an example, in the works cited before [34], [35], [37], erbium is responsible for the pump absorption and energy transfer to other REs (i.e., thulium and holmium), so its ability to contribute to the emission is reduced, due to a difficult optimization of its properties of both emitter and pump absorber. In the past, co-doping with ytterbium has been demonstrated as an efficient way to decouple pump absorption (i.e., made by ytterbium) with emission and gain properties of erbium or other REs [34], [39], [40]. In particular, erbium concentration can be optimized in terms of emission and gain and not for efficient 980-nm pump absorption [39], [40]. A further effect of co-doping and energy transfer processes is the transfer and filtering of the pump noise to the emitting level. This is an important parameter where stable emission is required [41], and a preliminary investigation is worthwhile.

Received 30 August 2024; revised 14 November 2024; accepted 23 November 2024. Date of publication 2 December 2024; date of current version 17 March 2025. This work was supported in part by the Starting Grant of Politecnico di Torino under Grant51_RIF20ST and in part by 51_RSG20ST "Attrazione e retenzione di docenti di qualità" under grant di Intesa Sanpaolo S.p.A. *(Corresponding author: Riccardo Ballarini.)*

The authors are with the Department of Electronics and Telecommunications, Politecnico di Torino, 10129 Turin, Italy (e-mail: riccardo.ballarini@polito.it; stefano.taccheo@polito.it).

Color versions of one or more figures in this article are available at https://doi.org/10.1109/JLT.2024.3509995.

Digital Object Identifier 10.1109/JLT.2024.3509995

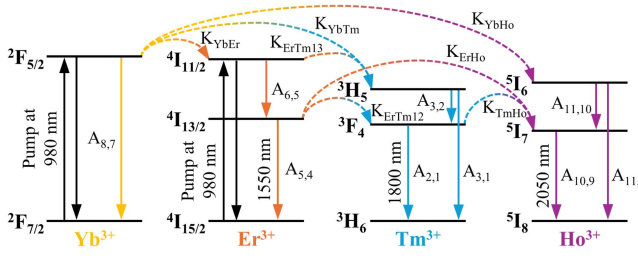

Fig. 1. Energy level scheme considered in this work for the germanate glass doped with Yb^{3+}, Er^{3+}, Tm^{3+} and Ho^{3+}. Black solid arrows represent the interactions with the pump, colored solid arrows represent the spontaneous decays, while dashed arrows represent the energy transfers.

In this paper, for the first time to our knowledge, we focus and investigate a quadruply-doped glass in terms of emission and gain spectra, and pump noise transfer functions. We note that in a previous paper [42] a specific possible device, a multi-wavelength laser, was numerically investigated. However, no investigation about the interplay between the different REs or about the general glass emission, gain and noise features was developed. In detail, the glass under investigation consists of a 980-nm-pumped germanate glass doped with Yb^{3+}, Er^{3+}, Tm^{3+} and Ho^{3+}. Germanium (Ge) has been chosen as hosting glass thanks to its interesting properties, in particular the high RE solubility and the wide optical transmission window (up to 5 μm) [34], [43], [44], [45], [46]. The idea is that the pump at 980 nm interacts mainly with ytterbium, which is the main pump absorber, but also with erbium. The pump excitation is transferred from ytterbium and erbium to the other two REs, as well as from ytterbium to erbium, via energy transfer processes, as shown in Fig. 1. So, in this glass ytterbium is the main pump absorber, while erbium, thulium and holmium are responsible for the emission, that could efficiently cover a wavelength range from 1500 nm to 2100 nm and beyond [32], [33], [34]. The presence of multiple inter-ion processes makes not trivial the design of such a glass. In order to optimize the properties of the quadruply-doped germanate glass, we used a suitable numerical model that simulates a bulk glass; in a future work, we will investigate the properties of optimized fiber active devices. The model is also able to compute the pump noise transfer function, in order to evaluate the pump noise effect and to assess if there are issues with the amplitude stability due to the complex interaction system [41]. This paper is organized as follow: the first section introduces the numerical model, the second one studies and optimizes the emission and the gain spectra, the last one shows and describes the pump noise transfer functions.

II. Numerical Model

The numerical model used to simulate the germanate glass doped with Yb^{3+}, Er^{3+}, Tm^{3+} and Ho^{3+} and pumped at 980 nm is based on the energy level scheme shown in Fig. 1, which was previously used to design a multi-wavelength fiber laser [42]. In Fig. 1, dashed arrows between ions indicate energy transfer processes and solid arrows spontaneous decays by photon or phonon emission. Any other energy level, energy transfer process, quenching effect, or upconversion process has been considered negligible [42] for the purpose of this model and the results discussed in this paper. We investigate the emission and gain properties of main laser transitions: erbium $^4I_{13/2}\rightarrow{}^4I_{15/2}$, thulium $^3F_4\rightarrow{}^3H_6$, and holmium $^5I_7\rightarrow{}^5I_8$. The eleven energy level system includes: three energy levels for thulium ($^3H_6$, $^3F_4$, $^3H_5$), three for erbium ($^4I_{15/2}$, $^4I_{13/2}$, $^4I_{11/2}$), two for ytterbium ($^2F_{7/2}$ and $^2F_{5/2}$), and three for holmium ($^5I_8$, $^5I_7$, $^5I_6$) (Fig. 1) [42]. The overall system of eleven non-linear differential equations is reported below (1a)–(1k), with the numeration of the levels that follows the order above (i.e., #1 is thulium $^3H_6$ and #11 is holmium $^5I_6$) [42], [47]:

$$\frac{\partial N_1}{\partial t} = +A_{2,1}N_2 + A_{3,1}N_3 - K_{YbTm}N_1N_8 + K_{TmHo}N_2N_9 - K_{ErTm13}N_1N_6 - K_{ErTm12}N_1N_5 \quad (1a)$$

$$\frac{\partial N_2}{\partial t} = +A_{3,2}N_3 - A_{2,1}N_2 - K_{TmHo}N_2N_9 + K_{ErTm12}N_1N_5 \quad (1b)$$

$$\frac{\partial N_3}{\partial t} = -A_{3,2}N_3 - A_{3,1}N_3 + K_{YbTm}N_1N_8 + K_{ErTm13}N_1N_6 \quad (1c)$$

$$\frac{\partial N_4}{\partial t} = -W_{4,6}N_4 + W_{6,4}N_6 + A_{6,4}N_6 + A_{5,4}N_5 - K_{YbEr}N_4N_8 + K_{ErHo}N_5N_9 + K_{ErTm13}N_1N_6 + K_{ErTm12}N_1N_5 \quad (1d)$$

$$\frac{\partial N_5}{\partial t} = +A_{6,5}N_6 - A_{5,4}N_5 - K_{ErHo}N_5N_9 - K_{ErTm12}N_1N_5 \quad (1e)$$

$$\frac{\partial N_6}{\partial t} = +W_{4,6}N_4 - W_{6,4}N_6 - A_{6,5}N_6 - A_{6,4}N_6 + K_{YbEr}N_4N_8 + K_{ErTm13}N_1N_6 \quad (1f)$$

$$\frac{\partial N_7}{\partial t} = -W_{7,8}N_7 + W_{8,7}N_8 + A_{8,7}N_8 + K_{YbEr}N_4N_8 + K_{YbHo}N_8N_9 + K_{YbTm}N_1N_8 \quad (1g)$$

$$\frac{\partial N_8}{\partial t} = +W_{7,8}N_7 - W_{8,7}N_8 - A_{8,7}N_8 - K_{YbEr}N_4N_8 - K_{YbHo}N_8N_9 - K_{YbTm}N_1N_8 \quad (1h)$$

$$\frac{\partial N_9}{\partial t} = +A_{10,9}N_{10} + A_{11,9}N_{11} - K_{YbHo}N_8N_9 - K_{ErHo}N_5N_9 - K_{TmHo}N_2N_9 \quad (1i)$$

$$\frac{\partial N_{10}}{\partial t} = -A_{10,9}N_{10} + A_{11,10}N_{11} + K_{ErHo}N_5N_9 + K_{TmHo}N_2N_9 \quad (1j)$$

$$\frac{\partial N_{11}}{\partial t} = -A_{11,10}N_{11} - A_{11,9}N_{11} + K_{YbHo}N_8N_9 \quad (1k)$$

TABLE I
CONSTANTS TAKEN FROM LITERATURE AND USED IN THE NUMERICAL MODEL

Parameter	Value	Description
τ_2	2.67 ms [53]	$^3F_4$ lifetime
τ_3	1.70 ms [53]	$^3H_5$ lifetime
τ_5	10.00 ms [54]	$^4I_{13/2}$ lifetime
τ_6	2.00 µs [54]	$^4I_{11/2}$ lifetime
τ_8	1.00 ms [54]	$^2F_{5/2}$ lifetime
τ_{10}	9.67 ms [55]	$^5I_7$ lifetime
τ_{11}	5.41 ms [55]	$^5I_6$ lifetime
$\beta_{3,1}$	99.05 % [53]	$^3H_5 \rightarrow {}^3H_6$ branching ratio
$\beta_{3,2}$	0.95 % [53]	$^3H_5 \rightarrow {}^3F_4$ branching ratio
$\beta_{6,4}$	≈ 0.00 % [42]	$^4I_{11/2} \rightarrow {}^4I_{15/2}$ branching ratio
$\beta_{6,5}$	≈ 100.00 % [42]	$^4I_{11/2} \rightarrow {}^4I_{13/2}$ branching ratio
$\beta_{11,9}$	84.20 % [55]	$^5I_6 \rightarrow {}^5I_8$ branching ratio
$\beta_{11,10}$	15.80 % [55]	$^5I_6 \rightarrow {}^5I_7$ branching ratio
K_{ErHo}	4×10^{-22} m^3s^{-1} [42]	$Er^{3+} \rightarrow Ho^{3+}$ energy transfer
K_{ErTm12}	4×10^{-22} m^3s^{-1} [42]	$Er^{3+} \rightarrow Tm^{3+}$ energy transfer
K_{ErTm13}	4×10^{-22} m^3s^{-1} [42]	$Er^{3+} \rightarrow Tm^{3+}$ energy transfer
K_{TmHo}	4×10^{-22} m^3s^{-1} [42]	$Tm^{3+} \rightarrow Ho^{3+}$ energy transfer
K_{YbEr}	4×10^{-22} m^3s^{-1} [42]	$Yb^{3+} \rightarrow Er^{3+}$ energy transfer
K_{YbHo}	4×10^{-22} m^3s^{-1} [42]	$Yb^{3+} \rightarrow Ho^{3+}$ energy transfer
K_{YbTm}	4×10^{-22} m^3s^{-1} [42]	$Yb^{3+} \rightarrow Tm^{3+}$ energy transfer
$\sigma_{1,2}$(1800 nm)	2.27×10^{-25} m^2 [49]	Tm Absorption cross section
$\sigma_{2,1}$(1800 nm)	6.30×10^{-25} m^2 [49]	Tm Emission cross section
$\sigma_{4,5}$(1550 nm)	1.65×10^{-25} m^2 [48]	Er Absorption cross section
$\sigma_{5,4}$(1550 nm)	2.77×10^{-25} m^2 [48]	Er Emission cross section
$\sigma_{4,6}$(980 nm)	7.00×10^{-25} m^2 [54]	Er Absorption cross section
$\sigma_{6,4}$(980 nm)	7.00×10^{-25} m^2 [54]	Er Emission cross section
$\sigma_{7,8}$(980 nm)	1.20×10^{-24} m^2 [54]	Yb Absorption cross section
$\sigma_{8,7}$(980 nm)	1.20×10^{-24} m^2 [54]	Yb Emission cross section
$\sigma_{9,10}$(2050 nm)	1.08×10^{-25} m^2 [50]	Ho Absorption cross section
$\sigma_{10,9}$(2050 nm)	3.65×10^{-25} m^2 [50]	Ho Emission cross section

where N_i is the *i*-level population, K is the energy transfer coefficient between two different REs (Fig. 1), $A_{i,j}$ is the radiative decay rate of the i→ j transition (Fig. 1) and it is given by $A_{i,j} = \beta_{i,j} / \tau_i$ (where $\beta_{i,j}$ is the branching ratio of that transition and τ_i is the time constant of the *i*-level); $W_{i,j}$ is the i→ j transition rate related to the pump and it is given by [42]:

$$W_{i,j} = \frac{\sigma_{i,j}(\lambda_p)}{h\frac{c_0}{\lambda_p}} P_p \frac{\Gamma_p}{A_d} \tag{2}$$

where $\sigma_{i,j}(\lambda_p)$ is the cross section at the pump wavelength λ_p (i.e., 980 nm), h is the Planck constant, c_0 is the speed of light in vacuum, P_p is the pump power, Γ_p is the overlap factor between doped region of area A_d and pump profile. Table I resumes all the parameters present in the rate equation model (1a)–(1k) and the references of the paper they have been taken from. The cross sections taken from literature [48], [49], [50] have been rescaled using the Füchtbauer-Ladenburg equation [51]. In all the results reported in this paper, Γ_p is 1, A_d is 78.5 μm^2 and P_p is 10 mW. Fig. 2 shows the calculated normalized population of the eleven energy levels at different pump power values using the parameters of Table I and a set of concentrations taken from literature [52]: 5.1×10^{25} ions m^{-3} of ytterbium, 1.7×10^{25} ions m^{-3} of erbium, 4.25×10^{24} ions m^{-3} of thulium and 4.25×10^{24} ions m^{-3} of holmium.

III. ION CONCENTRATION OPTIMIZATION

The glass under investigation could be able to emits and amplifies in a potential wavelength range from 1450 nm to 2150 nm [32], [33], [34], [48], [49], [50] thanks to the contribution of erbium, thulium and holmium; however, the optimization of the spectrum and its homogeneity is not trivial and depends on the mutual ion concentration ratios. The algorithm uses an initial set of concentrations taken from literature [52]: 5.1×10^{25} ions m^{-3} of ytterbium, 1.7×10^{25} ions m^{-3} of erbium, 4.25×10^{24} ions m^{-3} of thulium and 4.25×10^{24} ions m^{-3} of holmium. We fixed the concentration of ytterbium, while the concentrations of the emitting ions were changing by one order of magnitude up and down (e.g., erbium from 1.7×10^{24} ions m^{-3} to 1.7×10^{26} ions m^{-3}; thulium and holmium have been kept equal, so the overall degrees of freedom of the system were just two and meaningful figures could be produced to get insight into the ions interaction. In the end, we will comment about the effect of unbalancing thulium and holmium. The model investigates the population distribution in each of the eleven energy levels, in order to understand the role of all parameters.

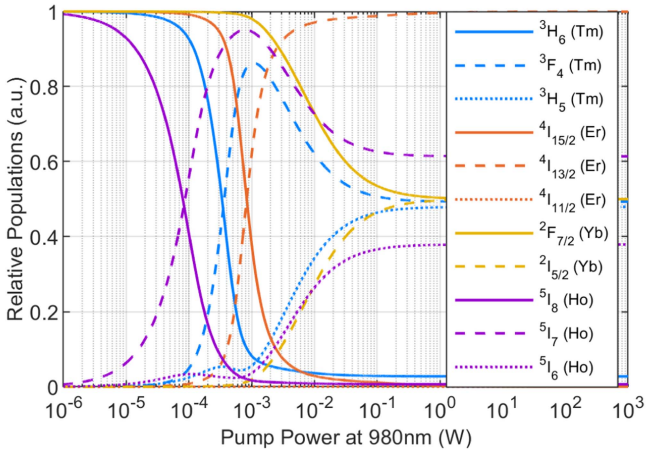

Fig. 2. Populations of the different energy state levels, normalized by the total concentration of each RE, at different pump power values.

In this section, the system has been studied and evaluated by means of several output parameters which are discussed in the following subsections: population reached in the emission energy level (ions m^{-3}), pumping efficiency, i.e. the population in the emission level as a percentage over the whole concentration, photon emission rate (ions m^{-3} s^{-1}), spontaneous emission spectrum (a.u.), as benchmark for ASE source applications, and gain spectrum (dB m^{-1}). All these parameters have been calculated for the emission levels in which we are interested: erbium $^4I_{13/2}$, thulium $^3F_4$ and holmium $^5I_7$.

A. Emission Level Population

Fig. 3 shows the populations of the emission levels, N_{RE}, where RE is one of the three emitting REs. Fig. 3(a) shows that erbium population depends almost exclusively on its own concentration, highlighting that with these concentrations erbium is high enough not to be quenched by thulium and holmium. Instead, thulium and holmium populations increase as both their concentrations or erbium concentration grow (Fig. 3(b) and (c); the dependence from the erbium concentration is due to the important energy transfer from erbium to thulium and

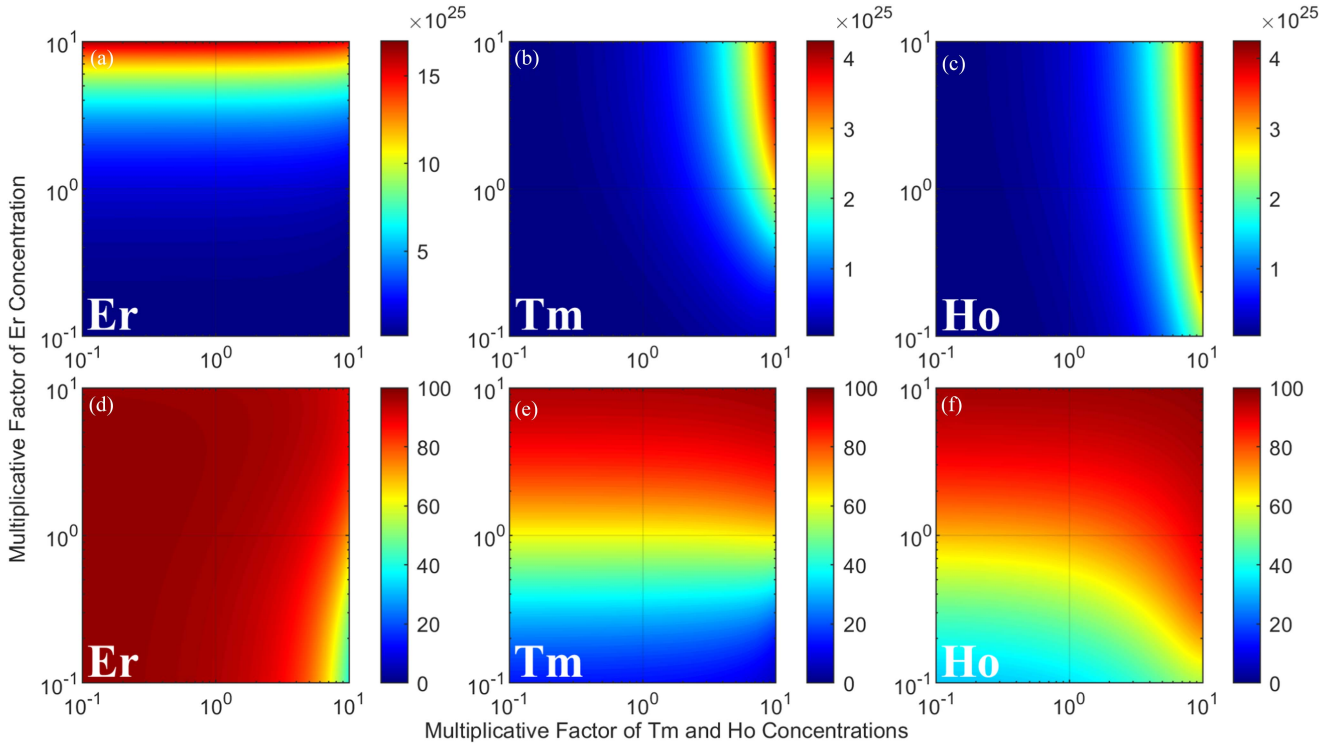

Fig. 3. (a)–(c) Population (ions m^{-3}) in the energy level (a) $^4I_{13/2}$ of Er, (b) $^3F_4$ of Tm, and (c) $^5I_7$ of Ho. (d-f) Population pumping efficiency (%) of the energy level (d) $^4I_{13/2}$ of Er, (e) $^3F_4$ of Tm, and (f) $^5I_7$ of Ho. Vertical axes represent the multiplicative factor applied to Er concentration, from 0.1 to 10, while the horizontal axes the multiplicative factor for Tm and Ho concentrations.

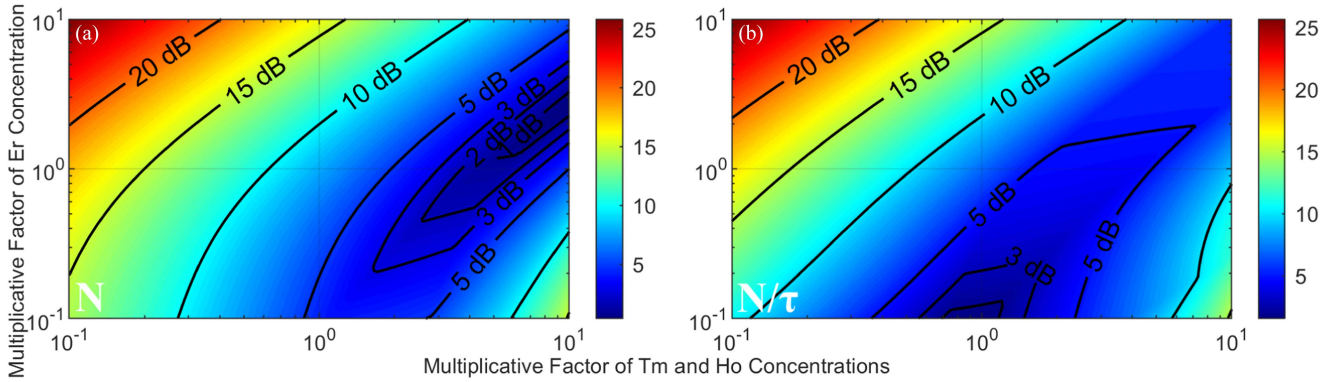

Fig. 4. (a), (b) Highest difference (dB) between (a) the populations in the energy levels $^4I_{13/2}$ of Er, $^3F_4$ of Tm and $^5I_7$ of Ho, and (b) the photon emission rates in the energy levels $^4I_{13/2}$ of Er, $^3F_4$ of Tm and $^5I_7$ of Ho. Vertical axes represent the multiplicative factor applied to Er concentration, from 0.1 to 10, while the horizontal axes the multiplicative factor for Tm and Ho concentrations.

holmium. In addition, Fig. 3(b) shows that thulium population is lower than holmium (Fig. 3(c)) at low erbium concentration level, highlighting that holmium exhibits a quenching effect on thulium if there is not enough erbium to pump it. Lastly, Fig. 4(a) represents the highest difference in dB between the populations of the three REs (i.e., the highest difference between Fig. 3(a)–(c). Fig. 4(a) shows that the sets of concentrations with the lowest difference in the populations lie in a diagonal area located on the right side of the graph, where the difference between the concentrations of erbium and thulium and holmium is lower than the initial condition. Instead, the area with the highest difference lies in the top left corner as expected, because there the erbium amount is too high in comparison to thulium and holmium.

B. *Emission Level Pumping Efficiency*

The pumping efficiency has been defined as:

$$\overline{N}_{RE} = \frac{N_{RE}}{N_{RE,tot}} 100 \tag{3}$$

where $\overline{N}_{RE}$ is the population of the RE emission level, N_{RE}, normalized to the total number of ions of that RE $N_{RE,tot}$, in percentage. Fig. 3(d)–(f) show the population pumping

efficiency, i.e. the populations reported in 3(a)–3(c) divided by the concentration of each RE. Erbium excitation efficiency is always close to 100%, with the only exception in the bottom right corner, where it has the lowest concentrations while thulium and holmium have the highest concentrations (Fig. 3(d)). Thulium excitation efficiency depends almost exclusively on erbium concentration (Fig. 3(e)), since thulium is mainly pumped by erbium. Instead, holmium excitation efficiency depends not only on erbium concentration, but also on thulium one (Fig. 3(f)), highlighting that holmium is pumped by both erbium and thulium. However, with enough erbium, all the three REs almost saturate to 100% (i.e., all the ions in the emission energy level state).

C. Photon Emission Rate

Photon emission rate, i.e. the number of photons emitted per unit of time and per unit of volume by each RE, has been defined as:

$$N_{photon,RE} = \frac{N_{RE}}{\tau_{RE}} \tag{4}$$

where $N_{photon,RE}$ is the photon emission rate (ions m^{-3} s^{-1}) and τ_{RE} is the time constant of energy level considered. The graphs of photon emission rates of the three REs are not reported here, because they are very similar to graphs of Fig. 3(a)–(c), except obviously for the values on the scale of the color bar. In fast, they are obtained from them by just dividing each RE by its own emission level lifetime value. Fig. 4(b) reports the highest difference in dB between the photon rates of the three REs; the graph is very similar to Fig. 4(a), but with a difference, the shift of the 3dB area towards lower concentrations, due to the higher holmium time constant respect to the thulium one, that further reduce holmium values versus erbium and thulium. While apparently small, Fig. 4(b) shows that photon emission rate optimization requires far lower concentration than emission level population optimization (Fig. 4(a)). This optimization is, for example, relevant to ASE source design.

D. Spontaneous Emission Spectrum

To evaluate the spontaneous emission spectral properties we used the following definition, which is used to describe the spontaneous emission term in active fiber devices [47]:

$$P_{SE,RE}(\lambda) = \frac{2\,h\,c_0^2}{\lambda^3} N_{RE}\,\sigma_{e,RE}(\lambda) \tag{5}$$

where $P_{SE,RE}$ is the spontaneous emission spectral density, as a function of the wavelength λ, per unit of length of the active material [47], h is the Planck constant, and $\sigma_{e,RE}$ is the emission cross section of the emission energy level considered. Therefore, $P_{SE,RE}$ is the power emitted over a given wavelength interval per unit of length of the active material. The dimensions in the International System are W m^{-2}, but in Fig. 5 we have reported the spectral power emitted in a 1-nm wavelength interval per unit of length: W/nm m^{-1}; Fig. 5(d) is in logarithmic scale, so the unit is dBm/nm m^{-1}. The area below each curve represents the total spontaneous emission power emitted per unit of length in W m^{-1}.

As before, spontaneous emission graphs for each RE are not reported, since they are very similar to the ones in Fig. 3(a)–(c). Fig. 5(a) shows the highest difference between the spontaneous emissions of the three REs, computed at 1550 nm for the erbium, at 1800 nm for the thulium, and at 2050 nm for the holmium; the area with the lowest difference is very similar to the previous graphs (i.e., Fig. 4(a), (b). Fig. 5(b) shows the spontaneous emission spectrum in the lowest point of Fig. 5(a) (white marker "b"); in this case, thulium and holmium alone are almost equal, but, since they are quite overlapped, the emission around 1950 nm is quite high in the overall spectrum. The noise on the side of erbium curve is not due to the numerical model, but was already present in the cross section digitized [48]. However, the emission spectrum of Fig. 5(b) has been taken from the area with low erbium concentration of Fig. 5(a). In order to increase the emission intensity, a set of concentrations from the top right corner of Fig. 5(a) should be taken, where the RE content in the glass is higher. Fig. 5(c) shows the spontaneous emission spectrum with a different set of concentrations (white "c,d" marker in Fig. 5(a): the multiplicative factor is 2.5 for erbium and 9 for thulium and holmium, resulting in a set of concentrations of 5.1×10^{25} ions m^{-3} of ytterbium, 4.25×10^{25} ions m^{-3} of erbium, 3.83×10^{25} ions m^{-3} of thulium and 3.83×10^{25} ions m^{-3} of holmium). In order to optimize the emission bandwidth, we selected a set of concentrations whereby the holmium contribution is lower, resulting in a more balanced shape, and the overall spectrum cover a -10 dB bandwidth of 660 nm, from 1471 nm to 2131 nm (Fig. 5(d)). Moreover, the power spectral density in this point (Fig. 5(c)) is one order of magnitude higher than the one in Fig. 5(b). This difference highlights the importance of balancing not only the spectral bandwidth but also the emission power. There are two main differences compared to the starting concentrations: erbium, thulium and holmium concentrations are now closer to the ytterbium one, and the erbium over thulium or holmium ratio is significantly lower, from 4 to 1.1, resulting in almost equal concentrations.

Fig. 5(e), (f) show how a variation in the concentrations affects the emission spectrum of Fig. 5(c). Fig. 5(e) shows the effect due to a variation of erbium concentration (along the vertical white line in Fig. 5(a)), while Fig. 5(f) shows the effect due to a variation of thulium and holmium concentrations (along horizontal white line in Fig. 5(a)). Fig. 5(e) shows that erbium emission grows almost proportionally with concentration increase, while thulium and holmium emission saturates, indicating that there is enough erbium to efficiently transfer excitation to thulium and holmium. Moreover, a higher content of erbium results in a much higher emission peak, at the cost of the spectral flatness. In Fig. 5(f) thulium and holmium emission grows proportionally to their concentration, while the erbium emission exhibits a little decrease, indicating that erbium concentration is again high enough not to be quenched by thulium and holmium.

Furthermore, we tested the system with unbalanced concentrations of thulium and holmium, by changing the Tm/Ho ratio (i.e., 1/5, 1/3, 1/2, 2, 3, 5). Fig. 6(a) shows an example with more holmium than thulium (i.e., Tm/Ho ratios of 1/5); in this

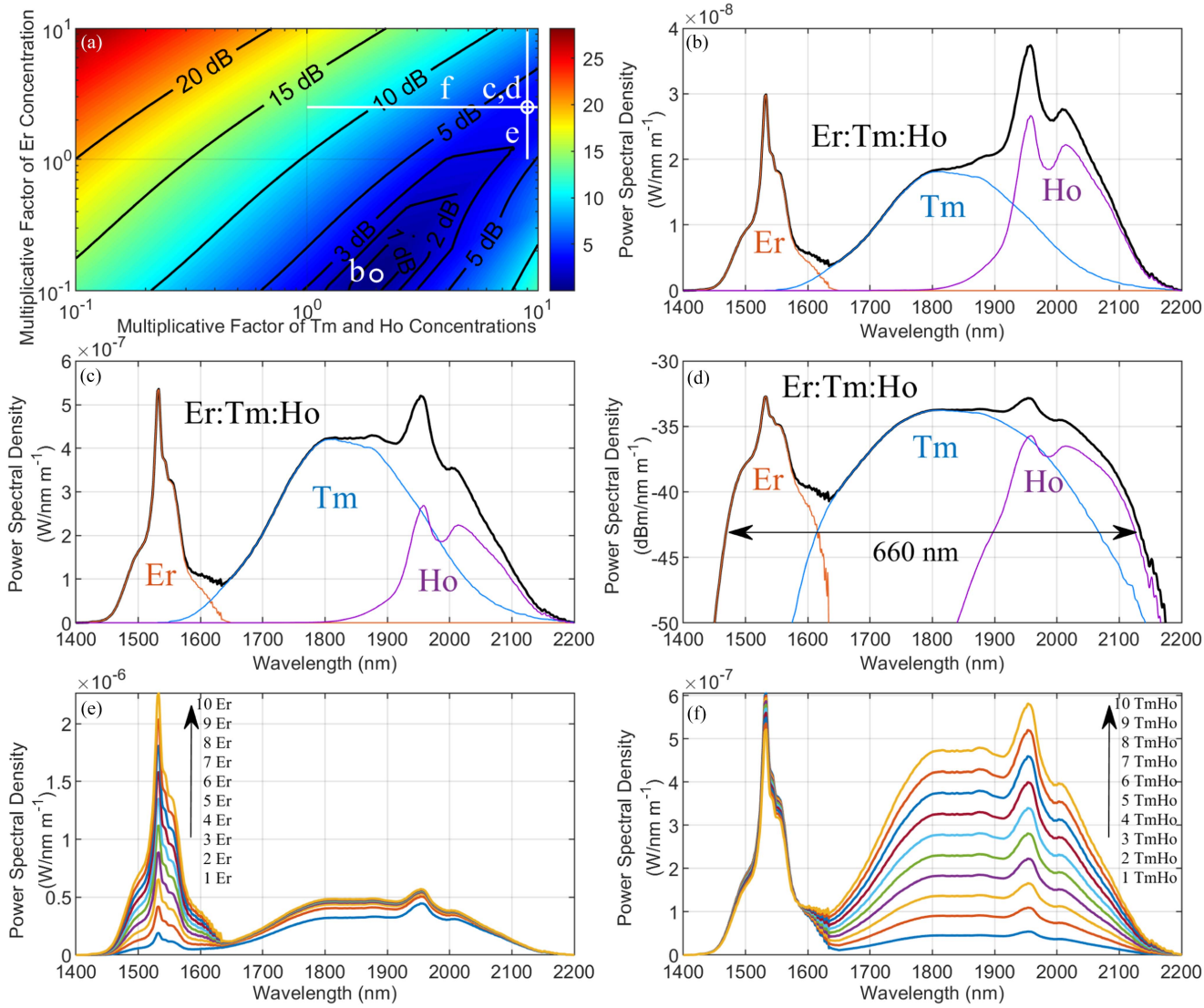

Fig. 5. (a) Highest difference (dB) between power spectral density of Er at 1550 nm, Tm at 1800 nm and Ho at 2050 nm. Vertical axis represents the multiplicative factor applied to Er concentration, from 0.1 to 10, while the horizontal axis the multiplicative factor for Tm and Ho concentrations. (b) Power spectral density spectrum with the REs concentration that guaranties the lowest difference ("b" marker in the first figure). (c), (d) Power spectral density spectrum with an optimal set of REs concentrations ("c,d" marker in the first figure), represented both (c) in W/nm m^{-1} and (d) in dBm/nm m^{-1}. (e) Power spectral density spectrum variation at different Er concentration (vertical white line "e" in the first figure). (f) Power spectral density spectrum variation at different Tm and Ho concentration (horizontal white line "f" in the first figure).

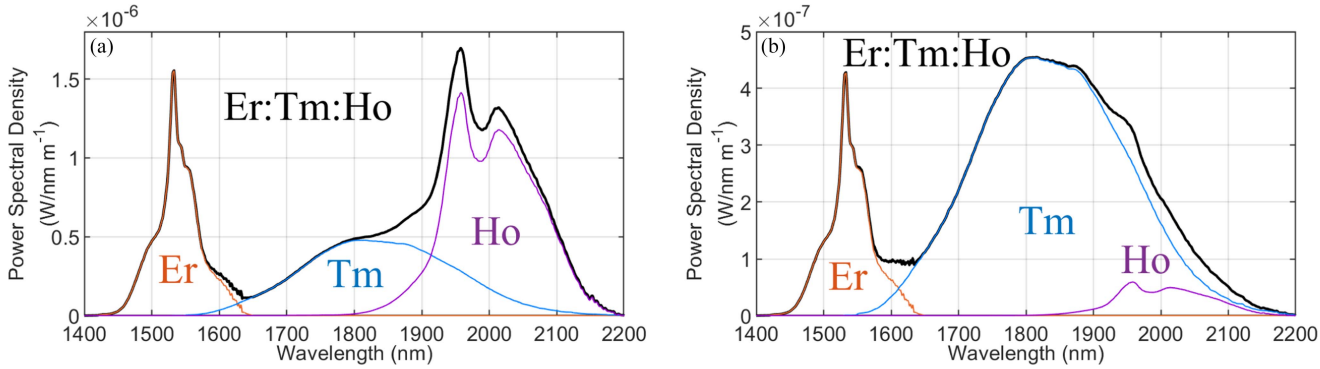

Fig. 6. (a) Power spectral density spectrum with Tm/Ho ratio of 1/5. (b) Power spectral density spectrum with Tm/Ho ratio of 5.

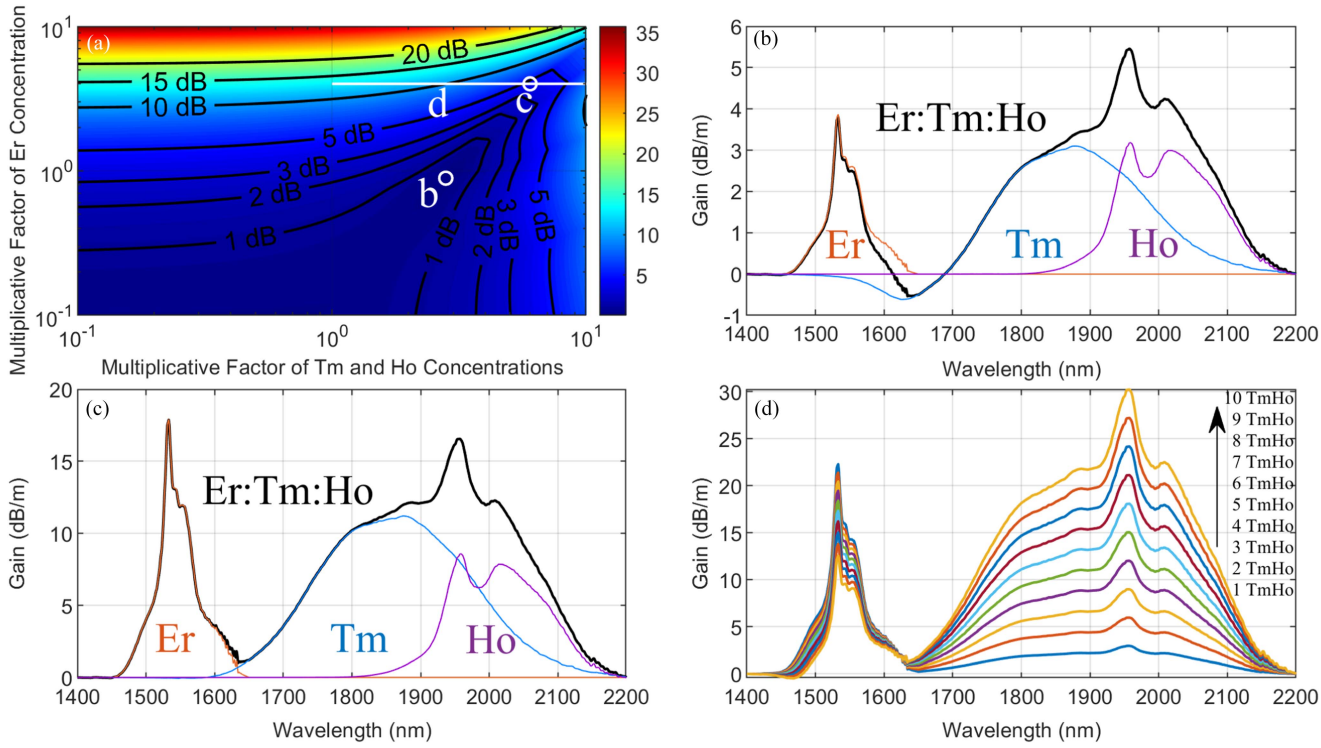

Fig. 7. (a) Highest difference (dB m^{-1}) between the gain of Er at 1550 nm, Tm at 1800 nm and Ho at 2050 nm. Vertical axis represents the multiplicative factor applied to Er concentration, from 0.1 to 10, while the horizontal axis the multiplicative factor for Tm and Ho concentrations. (b), (c) Gain spectra from (b) the set of REs concentrations with the lowest difference (white "b" marker) and (c) an optimal set (white "c" marker). (d) Gain spectrum variation at different Tm and Ho concentration (horizontal white line "d").

case, the emission spectrum exhibits a greater holmium peak, resulting in a less flat spectrum shape if compared to Fig. 5(c); indeed, the −10 dB flatness around 1600 nm cannot be achieved, due to both the high 1950 nm emission peak and the quenching effect of holmium toward thulium. In addition, there are neither advantages in terms of power spectral density, since it increases of barely 3dB in comparison to the ones in Fig. 5. Fig. 6(b) shows the opposite case (i.e., more thulium than holmium, Tm/Ho ratios of 5). As before, no advantages in terms of power spectral density can be observed. Moreover, the holmium emission is too low, resulting in a negligible holmium contribution, generating a small bandwidth reduction of 30 nm on the right side of the spectrum. Thus, the overall emission spectrum is composed only by erbium and thulium, failing the aim to merge erbium, thulium and holmium emissions. Therefore, the use of almost equal concentration of thulium and holmium offers the best properties.

E. Optical Gain

Gain coefficient has been defined as [42], [47], [56]:

$$g_{RE}(\lambda) = N_{RE}\,\sigma_{e,RE}(\lambda) - N_{RE,0}\,\sigma_{a,RE}(\lambda) \tag{6}$$

where g_{RE} is the gain coefficient, $N_{RE,0}$ is the population of the ground energy level, $\sigma_{e,RE}$ and $\sigma_{a,RE}$ are the emission and absorption cross sections. The graphs in this section (Fig. 7) report the gain in dB m^{-1}, defined as:

$$G_{RE}(\lambda) = 10\log_{10} e^{g_{RE}(\lambda)} \approx 4.343\, g_{RE}(\lambda) \tag{7}$$

The gain is reported in dB per unit of length (dB m^{-1}), but we remind that we are considering a single point emission which may likely not be kept over a long piece of fiber. In fact, the overall gain along a fiber is lower and with added unbalance due to different signal, pump and ASE power. The concentrations used to obtain Fig. 7 are lower (i.e., 1/5) than the ones in previous graphs; the initial concentrations used for the gain graphs (Fig. 7) are: 1.02×10^{25} ions m^{-3} of ytterbium, 3.4×10^{24} ions m^{-3} of erbium, 8.5×10^{23} ions m^{-3} of thulium and 8.5×10^{23} ions m^{-3} of holmium.

As before, single RE gain graphs are not shown since they are very similar to the population ones (Fig. 3(a)–(c). Fig. 7(a) reports the highest difference between gain values of the three REs, calculated at 1550 nm for erbium, at 1800 nm for thulium, and at 2050 nm for holmium. The lowest difference area is located in the same position as the other parameters, while the area with the highest difference covers almost all the top part, where the erbium has the highest concentration. Since erbium is almost totally inverted (Fig. 3(d)–(f), the erbium ground level population is very low, so if there is too much erbium, its gain is too high compared to other REs. Fig. 7(b) shows the gain spectrum with the concentrations from the lowest point of Fig. 7(a) (white "b" marker); in this condition, thulium is not enough inverted (Fig. 3(e)), so the gain is negative in a small band around 1600 nm, due to the thulium absorption cross section. Fig. 7(c) shows the gain spectrum with another set of concentrations (white "c" marker in Fig. 7(a)), that guarantees a better thulium inversion and thus a positive gain all over

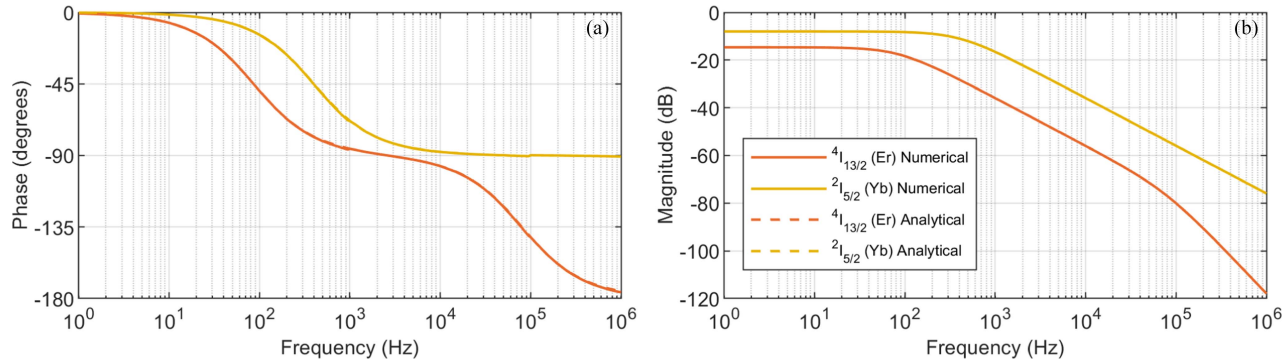

Fig. 8. (a), (b) Comparison between the transfer function (a) phase and (b) magnitude obtained with the analytical expression (dashed lines) and through the numerical model (solid line). The analytical functions are not visible because of the overlap with the numerical model results.

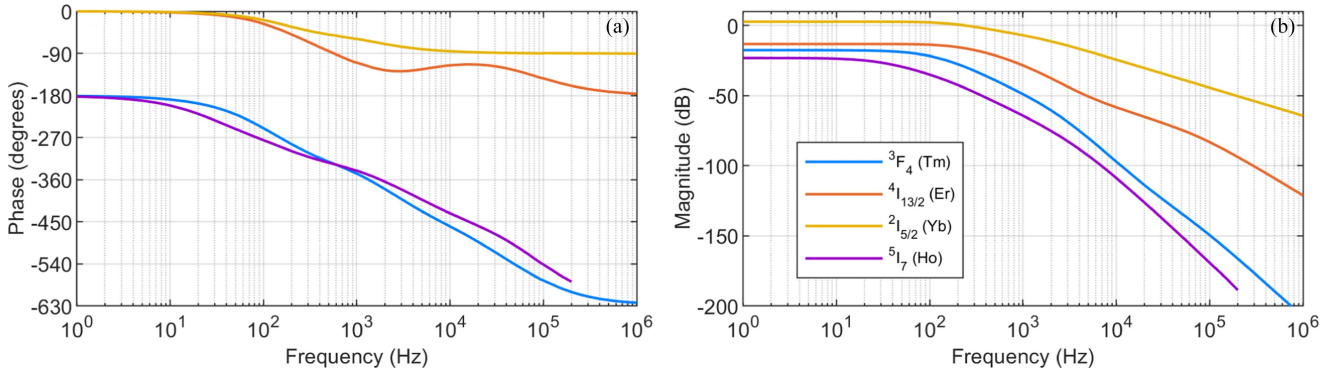

Fig. 9. (a), (b) Numerical transfer function (a) phase and (b) magnitude of the Yb^{3+}:Er^{3+}:Tm^{3+}:Ho^{3+} co-doped germanate glass with the set of concentrations that guaranties an optimal spontaneous emission (Fig. 5 c): 5.1×10^{25} ions m^{-3} of ytterbium, 4.25×10^{25} ions m^{-3} of erbium, 3.83×10^{25} ions m^{-3} of thulium and 3.83×10^{25} ions m^{-3} of holmium. Holmium lines have been truncated due to resolution issues of the numerical model.

the spectrum. Other than a better spectral homogeneity and a positive gain all over the spectrum, the gain in Fig. 7(c) is higher compared to Fig. 7(b). In this point, the multiplicative factor is 4 for erbium and 5.5 for thulium and holmium, resulting in a set of concentrations of 1.02×10^{25} ions m^{-3} of ytterbium, 1.36×10^{25} ions m^{-3} of erbium, 4.68×10^{24} ions m^{-3} of thulium and 4.68×10^{24} ions m^{-3} of holmium. As before, here erbium is higher than ytterbium, and the erbium over thulium or holmium ratio is lower than initial condition, from 4 to 2.9. Fig. 7(d) shows how a variation in the concentrations of thulium and holmium affects the gain spectrum of Fig. 7(c); thulium and holmium gain grow proportionally to their own concentration, while erbium gain exhibits a higher decrease respect to Fig. 5(f), with a small negative gain before 1500 nm at high thulium and holmium concentration. We tested the system by unbalancing thulium and holmium concentrations, again with not significant improvements.

IV. Transfer Function

The rate equations reported (1a)–(1k) form a non-linear differential equation system. This introduces a complex interplay of time dynamics and in particular a complex transfer of the pump intensity noise, affecting emission and gain temporal stability. In order to have a preliminary idea if this complex system of four REs may introduce noise degradation, we numerically evaluate the pump noise Transfer Functions (TF). To simulate dynamic conditions, the system has been solved using a fourth order Runge-Kutta (RK4) algorithm. In order to obtain the pump noise transfer function, a sinusoidal noise has been added to the pump power steady state value. The results reported in this section has been obtained with the peak-to-peak amplitude of the variation equal to 2% of the pump power (e.g., 0.2 mW if the pump power is 10 mW). We analyzed the frequency ranging from 1 Hz to 1 MHz, with a resolution of 20 steps per decade. The transfer function magnitude has been calculated as:

$$A_i = 20 \log_{10} \frac{\frac{\Delta N_i}{N_i}}{\frac{\Delta P}{P}} \tag{8}$$

where A_i is the transfer function magnitude of the *i*-level, ΔN_i is the peak-to-peak variation of the population N_i (the *i*-level population), and ΔP is the variation of the pump power P; as said before, $\Delta P/P$ is equal to 0.02. For the sake of clarity, we list the energy levels taken into account: $^2F_{5/2}$ (Yb), $^4I_{13/2}$ (Er), $^3F_4$ (Tm) and $^5I_7$ (Ho).

We compared analytical and numerical transfer functions for ytterbium and erbium to assess the correctness of the method over the wide frequency interval. The two REs were taken alone (single doping) and the analytical transfer function has been

obtained using Laplace transform [57]. Fig. 8 shows a perfect overlap between the numerical and the analytical solutions and confirms the assumption of small perturbation holds.

Fig. 9 shows the transfer function related to the pump intensity noise, considering the system with all the four REs and the set of concentrations that produced the best emission spectrum (i.e., 5.1×10^{25} ions m^{-3} of ytterbium, 4.25×10^{25} ions m^{-3} of erbium, 3.83×10^{25} ions m^{-3} of thulium and 3.83×10^{25} ions m^{-3} of holmium.). Fig. 9(b) shows that the transfer function magnitude exhibits a low-pass filter shape, attenuating high-frequency noise from the pump. Instead, Fig. 9(a) shows the phase graph, in which the position of the poles depends on the time constants and on the energy transfer coefficients; so, the transfer function of a glass could be used to fit experimental data, becoming an alternative tool to extract complex spectroscopic parameters (e.g., energy transfer coefficients and time constants). Instead, the presence of a zero in the erbium TF is representative of the energy transfer from ytterbium. We can conclude that the ytterbium improves the pumping efficiency and decouples the pump absorption from erbium, adding an extra step in transferring the pump noise to other REs; therefore, the system can be considered immune from pump intensity noise for frequency above few kHz. In addition, before reaching thulium and holmium, the pump noise is filtered firstly by ytterbium and then by erbium; so, thanks to the energy transfer processes, thulium and holmium are less sensitive to the pump noise, resulting in a low-pass-shape decaying with -60 dB per decade.

V. Conclusion

This paper numerically investigated, for the first time to our knowledge, the emission and gain properties of a 980-nm-pumped Yb^{3+}:Er^{3+}:Tm^{3+}:Ho^{3+} co-doped germanate glass. We showed that the properties depends on the relative RE concentrations, which influence the weight of direct pumping and excitation/de-excitation via the energy transfer processes among REs. A proper optimization of relative doping concentrations could provide a -10 dB flat emission spectrum in a wavelength range of above 650 nm, i.e. from 1471 nm to 2131 nm, and with a proper power spectral density. Potential applications could be tunable fiber lasers, or ASE fiber sources. Finally, considering the complex pumping processes involved, we analyzed the pump intensity noise impact on population level stability. We numerically calculated the transfer functions for the four REs, which show that additional filtering is provided by the transfer function processes.

Acknowledgment

The authors would like to thank A. M. Loconsole and Prof. F. Prudenzano of Politecnico di Bari, Italy.

References

[1] L. Reddy, "A review of the efficiency of white light (or other) emissions in singly and co-doped Dy^{3+} ions in different host (phosphate, silicate, aluminate) materials," *J. Fluorescence*, vol. 33, no. 6, pp. 2181–2192, 2023.

[2] Z. Hong et al., "Spectroscopic studies of Dy^{3+}3 ions doped gallium silicate glasses for yellow solid-state lasers," *Silicon*, vol. 16, no. 1, pp. 463–470, 2024.

[3] G. Zhang, H. Wang, S. Xu, F. Jia, H. Zhang, and C. Su, "Up-conversion color tunable and red luminescence of Ho3+/Yb3+ co-doped glass ceramics containing NaLaSio4 crystals," *J. Non-Crystalline Solids*, vol. 619, 2023, Art. no. 122567.

[4] J. Zmojda, M. Kochanowicz, P. Miluski, G. C. Righini, M. Ferrari, and D. Dorosz, "Investigation of upconversion luminescence in Yb3+ /Tm3+ /Ho3+ triply doped antimony-germanate glass and double-clad optical fiber," *Opt. Mater.*, vol. 58, pp. 279–284, 2016.

[5] X. Liu, B. Mei, and G. Tan, "Investigation of the sensitization effect of Yb3+ in Yb, Er co-doped Sr5(PO4)3F transparent ceramics: From single-band red upconversion to temperature sensing behavior," *J. Eur. Ceram. Soc.*, vol. 44, no. 13, pp. 7855–7866, 2024.

[6] S. D. Jackson, "Review of the fundamentals of energy transfer in metal-ion-doped crystals and glasses," *Opt. Mater.*, vol. 145, 2023, Art. no. 114405.

[7] J. Ding, C. Li, D. Zhao, L. Zhu, J. Li, and Y. Zhou, "Near-infrared luminescence property of Nd3+, Tm3+ and Er3+ doped tellurite glass," *Opt. Laser Technol.*, vol. 164, 2023, Art. no. 109459.

[8] P. Miluski et al., "Broadband profiled eye-safe emission of LMA silica fiber doped with Tm3+ /Ho3+ ions," *Materials*, vol. 16, no. 24, 2023, Art. no. 7679.

[9] Y. Chen et al., "Er–Tm co-doped materials for on-chip ultra-broadband waveguide amplifier," *Ceramics Int.*, vol. 50, no. 9, pp. 16398–16403, 2024.

[10] W. Cao et al., "Analysis of mid-infrared photoluminescence around 2.85 m in Yb3+ /Ho3+ co-doped synthetic silica-germanate glass," *Infrared Phys. Technol.*, vol. 89, pp. 363–368, 2018.

[11] K. Wang, X. Li, P. Wang, W. Hua, Z. Wang, and K. Han, "Broadband, continuous-wave, mid-infrared generation based on ASE fiber source," *Photonics*, vol. 9, 2022, Paper 724.

[12] W. Walasik, R. E. Tench, G. Rivas, J. M. Delavaux, and I. Farley, "1760 nm multi-watt broadband PM CW and pulsed Tm-doped fiber amplifier," *J. Lightw. Technol.*, vol. 41, no. 12, pp. 3916–3924, Jun. 2023.

[13] D. Li et al., "2-m-band single-frequency Tm/Ho co-doped fiber laser with several-Khz linewidth in 100 nm wavelength-tunable range," *Opt. Laser Technol.*, vol. 167, 2023, Art. no. 109766.

[14] B. Xie, F. Wei, K. Zhang, J. Chen, X. Feng, and S. Zhou, "Broadband near-infrared emission in bi-er co-doped germanosilicate glasses," *J. Non-Crystalline Solids*, vol. 624, 2024, Art. no. 122730.

[15] Y. Luo, B. Yan, J. Zhang, J. Wen, J. He, and G. D. Peng, "Development of bi/er co-doped optical fibers for ultra-broadband photonic applications," *Front. Optoelectron.*, vol. 11, pp. 37–52, 2018.

[16] X. Chen et al., "Enhanced gain characteristics of PbS-doped silica fiber in O-band by co-doping er ions," *IEEE Photon. J.*, vol. 15, no. 3, Jun. 2023, Art. no. 7201507.

[17] J. S. Wu, H. Hu, T. Du, and D. Yan, "A new industrial single-module 10kW fiber laser based on 915 nm wavelength pump source," *Proc. SPIE*, vol. 12169, pp. 1353–1358, 2022.

[18] M. Hemmati and M. J. Tafreshi, "Flexible biopolymer photodetectors based Er, Tb doped BaWo4@, CS for enhanced light-sensitive coatings," *Sensors Actuators A: Phys.*, vol. 375, 2024, Art. no. 115423.

[19] S. Zhou et al., "Upconversion luminescence of NaYF4: Yb3+, Er3+ for temperature sensing," *Opt. Commun.*, vol. 291, pp. 138–142, 2013.

[20] W. Xu, X. Gao, L. Zheng, Z. Zhang, and W. Cao, "An optical temperature sensor based on the upconversion luminescence from Tm3+ /Yb3+ codoped oxyfluoride glass ceramic," *Sensors Actuators, B: Chem.*, vol. 173, pp. 250–253, 2012.

[21] T. V. Huynh, H. L. Tran, N. T. N. Anh, and R. A. Doong, "Electrochemical sensor for rapid diagnosis and early-stage detection of pancreatic cancer using ER-GQDs decorated MoS2 nanoflowers," *Sensors Actuators B: Chem.*, vol. 413, 2024, Art. no. 135893.

[22] U. Pantulap, M. Arango-Ospina, and A. R. Boccaccini, "Bioactive glasses incorporating less-common ions to improve biological and physical properties," *J. Mater. Science: Mater. Med.*, vol. 33, pp. 1–41, 2022.

[23] C. J. White, S. R. Ramee, T. J. Collins, J. E. Mesa, and J. P. Murgo, "Holmium: YAG laser-assisted coronary angioplasty with multifiber delivery catheters," *Catheterization Cardiovasc. Diagnosis*, vol. 30, no. 3, pp. 205–210, 1993.

[24] T. Nagahashi et al., "Er: YAG laser-induced cavitation can activate irrigation for the removal of intraradicular biofilm," *Sci. Rep.*, vol. 12, no. 1, 2022, Art. no. 4897.

[25] B. Blagova, D. Krastev, N. Krastev, and L. Malinova, "Tissue changes and tissue reactivity following osteotomy by a conventional rotary device, an ultrasonic unit, and an Er: YAG laser–a comparative study in humans," *J. Stomatology, Oral Maxillofac. Surg.*, vol. 125, no. 5, 2024, Art. no. 101750.
[26] V. Molebny, P. McManamon, O. Steinvall, T. Kobayashi, and W. Chen, "Laser radar: Historical prospective—from the east to the west," *Opt. Eng.*, vol. 56, no. 3, 2016, Art. no. 031220.
[27] A. M. Volikova, I. A. Lobach, and S. I. Kablukov, "Laser vibrometer-rangefinder based on self-sweeping fiber laser," *Opt. Exp.*, vol. 30, no. 12, 2022, Art. no. 22025.
[28] S. Tanabe, "Rare-earth-doped glasses for fiber amplifiers in broadband telecommunication," *Comptes Rendus Chimie*, vol. 5, pp. 815–824, 2002.
[29] H. Lao et al., "Dual-stage double-pass extended L-band erbium-doped fiber amplifier with improved gain performance," *Photonics*, vol. 10, no. 11, 2023, Art. no. 1266.
[30] S. Zhang, Y. H. Dong, J. N. Zhang, X. B. Zhang, T. Y. Wang, and Y. Guo, "An erbium-doped fiber amplifier with tunable gain-clamping in the extended L-band," *IEEE Photon. Technol. Lett.*, vol. 36, no. 9, pp. 617–620, May 2024.
[31] X. Huang, S. Liang, L. Xu, D. J. Richardson, and Y. Jung, "Wideband (13.7 Thz) gain-flattened Yb-doped fiber amplifier for telecommunication applications," *IEEE Photon. Technol. Lett.*, vol. 36, no. 12, pp. 791–794, Jun. 2024.
[32] A. Albalawi, M. Kochanowicz, J. Zmojda, P. Miluski, D. Dorosz, and S. Taccheo, "Fluorescence spectrum of an Yb:Er:Tm:Ho doped germanate glass," in *Proc. OSA Laser Congr.*, 2018, pp. ATu2A–4.
[33] M. Kochanowicz, J. Zmojda, P. Miluski, D. Dorosz, and S. Taccheo, "Spectroscopy of an Yb:Er:Tm:Ho four-doped germanate glass for broadband amplification and lasing," in *Proc. OSA Laser Congr.*, 2019, pp. JTu3A–22.
[34] M. Kochanowicz et al., "Ultra-broadband emission in Er3+ /Tm3+ /Ho3+ triply-doped germanate glass and double-clad optical fiber," *Opt. Mater. Exp.*, vol. 12, no. 6, 2022, Art. no. 2332.
[35] X. Su et al., "Enhanced 1.80 m fluorescence in Er3+ /Yb3+ /Tm3+ tri-doped tellurite glass for fiber lasers," *J. Alloys Compounds*, vol. 739, pp. 149–159, 2018.
[36] L. Zhu, D. Zhao, C. Li, J. Ding, J. Li, and Y. Zhou, "Improved 2 m broadband luminescence in Tm^{3+} /Ho^{3+} doping tellurite glass," *Opt. Exp.*, vol. 31, 2023, Art. no. 12819.
[37] S. Liang, Z. Hou, G. Zhou, J. Liu, and C. Xia, "Broadband stimulated emission generation in Er^{3+} /Tm^{3+} /Ho^{3+} codoped optical fiber rod," *Opt. Eng.*, vol. 57, p. 1, 2018.
[38] Y. Tian, R. Xu, L. Hu, and J. Zhang, "Intense 2:7 m and broadband 2:0 m emission from diode-pumped Er^{3+} =Tm^{3+} =Ho^{3+} -doped fluorophosphate glass," *Opt Lett.*, vol. 36, no. 16, pp. 3218–3220, Aug. 15, 2011.
[39] P. Laporta, G. Sacchi, S. Taccheo, S. Longhi, and O. Svelto, "Diode-pumped microchip Er–Yb:glass laser," *Opt. Lett.*, vol. 18, no. 15, 1993, Art. no. 1232.
[40] G. D. Valle et al., "Single-mode and high power waveguide lasers fabricated by ion-exchange," *Opt. Exp.*, vol. 16, no. 16, pp. 12334–12341, Aug. 2008. [Online]. Available: https://opg.optica.org/oe/abstract.cfm?URI=oe-16-16-12334
[41] S. Taccheo, P. Laporta, O. Svelto, and G. D. Geronimo, "Lasers and optics theoretical and experimental analysis of intensity noise in a codoped erbium-ytterbium glass laser," *Appl. Phys. B*, vol. 66, no. 1, pp. 19–26, 1998.
[42] M. C. Falconi, D. Laneve, V. Portosi, S. Taccheo, and F. Prudenzano, "Design of a multi-wavelength fiber laser based on Tm:Er:Yb:ho co-doped germanate glass," *J. Lightw. Technol.*, vol. 38, no. 8, pp. 2406–2413, Apr. 2020.
[43] A. Jha et al., "Rare-earth ion doped TeO2 and GeO2 glasses as laser materials," *Prog. Mater. Sci.*, vol. 57, no. 8, pp. 1426–1491, 2012.
[44] M. Kochanowicz et al., "Analysis of upconversion luminescence in germanate glass and optical fiber codoped with Yb^{3+}/Tb^{3+}," *Appl. Opt.*, vol. 55, no. 9, 2016, pp. 2370–2374.
[45] M. Kochanowicz et al., "Structural and luminescent properties of germanate glasses and double-clad optical fiber co-doped with Yb^{3+}/Ho^{3+}," *J. Alloys Compounds*, vol. 727, pp. 1221–1226, 2017.
[46] M. Kochanowicz et al., "Tm^{3+}/Ho^{3+} co-doped germanate glass and double-clad optical fiber for broadband emission and lasing above 2 m," *Opt. Mater. Exp.*, vol. 9, 2019, Art. no. 1450.
[47] A. M. Loconsole, M. C. Falconi, V. Portosi, A. Annunziato, S. Taccheo, and F. Prudenzano, "Incoherent multi-wavelength emission in the wavelength range 1500-2100 nm," in *Proc. IEEE AEIT Int. Annu. Conf.*, 2021, pp. 1–6.
[48] T. Wei et al., "Optical spectroscopy and population behavior between $^4i_{11/2}$ and $^4i_{13/2}$ levels of erbium doped germanate glass," *Opt. Mater. Express*, vol. 4, no. 10, 2014, pp. 2150–2165.
[49] X. Wen et al., "Highly Tm^{3+} doped germanate glass and its single mode fiber for 2.0 μm laser," *Sci. Rep.*, vol. 6, no. 1, 2016, Art. no. 20344.
[50] A. Hemming, N. Simakov, J. Haub, and A. Carter, "A review of recent progress in holmium-doped silica fibre sources," *Opt. Fiber Technol.*, vol. 20, no. 6, pp. 621–630, 2014.
[51] R. Paschotta, "Füchtbauer—Ladenburg equation," *RP Photon. Encyclopedia Laser Phys.*, 2006, doi: 10.61835/xy1.
[52] M. C. Falconi, D. Laneve, V. Portosi, S. Taccheo, and F. Prudenzano, "Modeling of a 980-nm pumped Yb:Er:Tm:Ho co-doped glass device for homogeneous gain and lasing over a 600-nm wavelength interval," in *Proc. Adv. Solid State Lasers*, 2019, pp. JTu3A–31.
[53] R. R. Xu, Y. Tian, M. Wang, L. L. Hu, and J. J. Zhang, "Spectroscopic properties of 1.8 m emission of thulium ions in germanate glass," *Appl. Phys. B: Lasers Opt.*, vol. 102, pp. 109–116, 2011.
[54] S. Taccheo, G. Sorbello, S. Longhi, and P. Laporta, "Measurement of the energy transfer and upconversion constants in Er–Yb-doped phosphate glass," *Opt. Quantum Electron.*, vol. 31, pp. 249–262, 1999.
[55] R. Chen et al., "Thermal and luminescent properties of 2μm emission in thulium-sensitized holmium-doped silicate-germanate glass," *Photon. Res.*, vol. 4, pp. 214–221, 2016.
[56] A. M. Loconsole, M. C. Falconi, D. Laneve, V. Portosi, S. Taccheo, and F. Prudenzano, "Wideband optical amplifier based on Tm:Er:Yb:Ho co-doped germanate glass," in *Proc. IEEE Ital. Conf. Opt. Photon.*, 2020, vol. 9, pp. 1–4.
[57] P. A. Lynn, *The Laplace Transform and the Z-Transform*. London, U.K.: Macmillan Education, 1986, doi: 10.1007/978-1-349-18461-3_6.

Riccardo Ballarini received the M.S. degree in biomedical engineering from Politecnico di Torino, Turin, Italy, in 2020, where he is currently working toward the Ph.D. degree. After, he joined Leonardo S.p.A., Italy, as Software Engineer. He is author of one invited paper on medical applications of flexible photonics. His research interests include range from optical fiber lasers and amplifiers and rare-earth doped materials to biomedical applications of photonic techniques.

Stefano Taccheo was born in Trieste, Italy, in 1964. He received the degree in nuclear engineering from the Politecnico di Milano, Italy, in 1989, and the Ph.D. degree in applied physics from the Politecnico di Torino, Turin, Italy, in 1996. From 1990 to 1991, he was a Researcher with SIRTI and CSELT Turin, working on optical fiber amplifiers. From 1991 to 1996, he was a Researcher with the Centre of Quantum Electronic, National Research Council, Milan, with focus on diode pumped infrared bulk glass lasers. In 1997, he was a Visiting Researcher with the ORC, Southampton, U.K., on high-power fiber lasers. He was an Assistant Professor and Associate Professor with Politecnico di Milano, in 1998 and 2004, respectively. Main activity was on highly-doped waveguide lasers and amplifiers fabricated by ion-exchange technique or by direct writing using femtosecond pulses. In 1999, he spent a sabbatical year working on continuum fibre sources with the Lightwave Transmission Group, Lucent Bell Labs, U.S. In 2007, he joined the College of Engineering, Swansea University to set-up the Laser and Photonic group with the Mid-Infrared Laboratory and the Advanced Communication Laboratory and founded the joint Centre for Cosmetic and Curative applications of Compound Semiconductor Tech with Compound Semiconductor Centre Ltd. In 2019, he joined Politecnico di Torino, Turin, Italy. He is author of more than 250 journal and conference publications. His research interests include sources and applications to medicine, communication, and sensing. His research interests also include fibre lasers, MIR-sources, spectroscopy of new glasses and active materials, solid state lasers, optical amplifiers, continuum sources, and fibre-based optical components. He recently created and was appointed as the Director of CIBioF the Photonics InterUniversity Research Centre for the study of Pharmacological and Oncological Biomarkers. He is elected member of the Board of Stakeholder of Photonics21 from 2023 to 2026, he was also a Swansea Representative from 2017 to 2020. He has been a consultant of several laser and telecom companies and he has been the General Chair of OSA Advance Solid-State Lasers from 2019 to 2020 and was the Co-Chair for Materials. He is founder Co-Chair of SPIE Photonics Europe Fiber Lasers and Glass Photonics: Materials through Applications,since 2018. He chaired the H2020 Network COST MP1401 on fiber lasers and their applications. He was the co-recipient of the 1993 Philip Morris Prize (with Prof. Svelto and Prof. Laporta) for the first demonstration of the diode-pumped Er:Yb bulk glass laser.